CHEMISTRY
A EUROPEAN JOURNAL

Structure–Property Correlations in Solid Solutions of $(CuI)_8P_{12-x}As_x$, $2.4 \leq x \leq 6.6$

Buddhimathie Jayasekera,[a] Stephanie L. Brock,*[a] Andy Y. H. Lo,[b] Robert W. Schurko,[b] and Gholam-Abbas Nazri[b]

Abstract: A series of P/As mixed pnicogen phases of composition $(CuI)_8P_{12-x}As_x$, in which x = 2.4, 4.2, 4.8, 5.4, and 6.6, have been synthesized and characterized by X-ray single crystal and powder diffraction, solid-state NMR spectroscopy, thermal gravimetric analysis, and impedance spectroscopy. These materials are isostructural to $(CuI)_8P_{12}$ and consist of neutral, tubular P/As mixed pnicogen chains associated with Cu^I and I^- ions. The As is distributed throughout the pnicogen chains; however, the "roof" sites of the [P8] cage show preferred occupation by As relative to the other sites. Accordingly, the change in cell volume is not a linear function of the As incorporation. Solid-state ^{31}P NMR spectroscopy of the 40% As incorporated sample are consistent with the X-ray structural model, with extensive broadening due to ^{31}P–^{75}As coupling and site disorder, and a change in the chemical shifts of the resonances due to the As substitution into the lattice. The degree of copper ion site disorder, probed by single-crystal X-ray diffraction, increases with increasing As content. Although very little change is observed in the copper ionic conductivity of polycrystalline samples, which ranges from $1.8–5.1 \times 10^{-6}\,S\,cm^{-1}$ for $(CuI)_8P_{12-x}As_x$, $x = 0$, 4.2, 5.4; a single crystal ($x = 4.8$) measured along the needle axis has a conductivity of $1.7 \times 10^{-3}\,S\,cm^{-1}$ at 128 °C. This represents an order of magnitude improvement in conductivity over $(CuI)_8P_{12}$ at the same temperature.

Keywords: conducting materials · copper · impedance spectroscopy · NMR spectroscopy · pnicogens

Introduction

The copper–pnicogen–halides represent a relatively small class of compounds featuring infinite chains of phosphorus surrounded by Cu^I halide.[1] The number of existing phases in this distinctive class of compounds is extremely small, and hitherto only Cu-P-X (X = Br, I) compounds have been reported. These can be categorized into two classes, neutral ($(CuI)_8P_{12}$,[2] $(CuI)_2P_{14}$,[3] and $(CuI)_3P_{12}$[4]) and anionic ($Cu_3P_{15}I_2$[5] and $Cu_{12}P_{20}Br_{10}$[6]) based on the charge on the chains of phosphorus.[7] The former have Cu^I weakly associated with the neutral pnicogen chains and are known to demonstrate predominantly Cu^I ionic conductivity. In contrast, the latter have strong electrostatic interactions between copper ions and negatively charged phosphorus atoms that hinder the mobility of Cu^I ions, resulting in predominantly electronic conductivity.[7] Among the Cu-P-X compounds, $(CuI)_8P_{12}$, the most cuprous iodide-rich neutral phosphorus phase, has shown the best ionic conductivity to date: $\sigma = 1.90 \times 10^{-3}\,S\,cm^{-1}$ at 186 °C for a single crystal.[8] However, it is several orders of magnitude less than that of the best copper ion conductor known thus far, $Rb_4Cu_{16}I_7Cl_{13}$,[9] ($\sigma = 0.34\,S\,cm^{-1}$ at room temperature).

We sought to examine whether copper ion conductivity could be improved by tuning the pnicogen–copper interaction, specifically by incorporating larger, more polarizable pnicogens (As, Sb). Although the logical end products $(CuI)_8As_{12}$ and $(CuI)_8Sb_{12}$ do not appear to be stable, we discovered that solid solutions of P/As chains could be prepared and a new compound, $(CuI)_8P_{7.2}As_{4.8}$, in which 40% of P is substituted by As, has been reported.[10] This compound is isostructural to its parent compound, $(CuI)_8P_{12}$, consisting of alternating Pn_8 cages and Pn_4 planar squares

[a] B. Jayasekera, Prof. S. L. Brock
Department of Chemistry, Wayne State University
Detroit MI 48202 (USA)
Fax: (+1) 313-577-8822
E-mail: sbrock@chem.wayne.edu

[b] A. Y. H. Lo, Prof. R. W. Schurko, Prof. G.-A. Nazri
Department of Chemistry & Biochemistry
University of Windsor, 393 Essex Hall
Windsor, Ontario, N9B 3P4 (Canada)

Supporting information for this article is available on the WWW under http://www.chemeurj.org/ or from the author. The supporting information contains a description of how ^{31}P chemical shifts were arrived at and Arrhenius plots of the conductivity for $(CuI)_8P_{7.2}As_{4.8}$.

DOI: 10.1002/chem.200400727

(Pn = P/As) to produce $^{1}_{\infty}$([Pn8]Pn4(4)[]) polymeric tubes (according to nomenclature proposed by Böcker and Häser[11]). These 1D chains have a close similarity to the units found in Hittorf's violet modification of phosphorus[12] ($^{2}_{\infty}$([P8]P2[P9]P2[], Figure 1), but are surrounded by Cu^{I} and

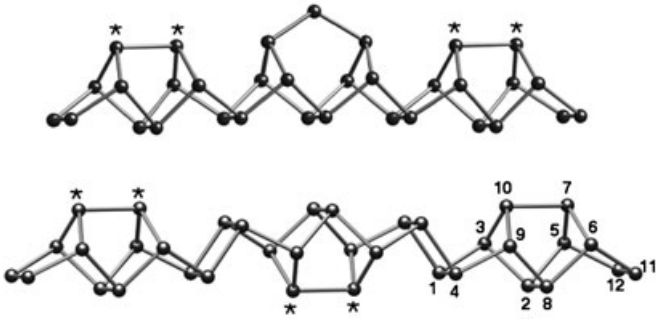

Figure 1. Structure of polyphosphorus chains: Top: a fragment from Hittorf's phosphorus; Bottom: a fragment of phosphorus chain from $(CuI)_8P_{12}$. The "roof" positions are noted with *.

iodide ions. Recently, it has been shown that the pnicogen chains in both $(CuI)_8P_{12}$ and $(CuI)_8P_{7.2}As_{4.8}$ can effectively be liberated from the CuI host by treatment with aqueous potassium cyanide, producing novel allotropes of phosphorus and binary P–As, respectively.[13,14]

Although each pnicogen position in $(CuI)_8P_{7.2}As_{4.8}$ has shared occupancy of both P and As, the "roof" positions in the [Pn8] cages (indicated by * in Figure 1) appear to be As rich, suggesting that these are not true solid solutions, but that there are preferred sites for As within the structure. Furthermore, the Cu^{I} lattice in the 40% As phase shows increased disorder relative to the parent compound, suggesting that As substitution may lead to augmented copper ion conductivity. Accordingly, we sought to prepare a series of compounds $(CuI)_8P_{12-x}As_x$, over the solid-solution range $12 > x > 0$, in order to assess the extent to which As can be incorporated, the degree of As ordering in the pnicogen chain, and the change in Cu^{I} ion conductivity upon As substitution. Herein we report a series of five P/As mixed pnicogen compounds with 20–55% As incorporation: $(CuI)_8P_{12-x}As_x$, in which $x = 2.4$, 4.2, 4.8, 5.4, and 6.6; and provide comparisons of their structural and physicochemical properties, with the intention of addressing the questions posed above.

Results and Discussion

Synthesis and composition of mixed pnicogen compounds—probing the limits of As incorporation: The ability to synthesize P/As mixed pnicogen compounds with As up to 40%[10] led us to question just how much As can in fact be substituted for P in $(CuI)_8P_{12}$; accordingly, syntheses of $(CuI)_8P_{12-x}As_x$ phases with As content up to 90% were carried out using conventional high-temperature ampoule techniques. Stoichiometric amounts of CuI, red P, and elemental As were ground together, pressed into a pellet, placed in an alumina boat, and heated at 550°C for two weeks in an evacuated fused silica jacket. The targeted stoichiometries were $(CuI)_8P_{10.8}As_{1.2}$ (10% As), $(CuI)_8P_{9.6}As_{2.4}$ (20% As), $(CuI)_8P_{7.8}As_{4.2}$ (35% As), $(CuI)_8P_{7.2}As_{4.8}$ (40% As), $(CuI)_8P_{6.6}As_{5.4}$ (45% As), $(CuI)_8P_{5.4}As_{6.6}$ (55% As), $(CuI)_8P_{4.8}As_{7.2}$ (60% As), and $(CuI)_8P_{1.2}As_{10.8}$ (90% As).

During the reactions, vapor-phase transport occurred, resulting in well-formed crystals at the colder parts of the ampoule. To facilitate transport, the pellet (reactants) was placed nearest to the thermocouple to generate a temperature gradient of approximately 40°C. In most of the reactions, the pellet residue was also covered with crystals. The crystals are dark with a metallic luster and form as flat needles, similar to those of $(CuI)_8P_{12}$. It was difficult to produce a substantial amount of transported crystals from the low As compositions (10% and 20% As) even upon recrystallization. On the other hand, the major product of the 40% and 45% As reactions is bundles of crystals, formed after a two-week heating cycle. There is also a rough correlation of crystal size with the degree of As incorporation; small crystals, about 1–3 mm in length, form for 10% and 20% As compositions, whereas fairly long crystals, approximately 3–10 mm, are obtained from the 40% and 45% As stoichiometries.

Powder X-ray diffraction (PXRD) of the ground products revealed the presence of elemental As in 60% and 90% As compositions, whereas no elemental As was detected for compositions with a lower percentage of As. To verify the compositional region at which phase separation occurs, reactions with 55% and 60% As were repeated, and again, signals of elemental As were detected by PXRD only in the 60% As composition. This suggests that the solubility of As in the mixed pnicogen polymer is exceeded in the region between 55 and 60% As. Thus, despite the fact that neutral tubular polymers are unknown for As, and that no pure arsenic phase isostructural to $(CuI)_8P_{12}$ exists, high amounts of As can be stabilized within the chains in the presence of phosphorus.

The PXRD patterns of ground crystals for compositions up to and including 55% As feature narrow peaks of full-width at half maximum height (FWHM) ~0.1°, suggesting the presence of a single-phase material, with a pattern similar to that of $(CuI)_8P_{12}$. As expected, the peaks are shifted towards higher d spacings relative to the parent compound (Figure 2). The residual pellet has a similar pattern to that for the crystals, along with peaks corresponding to CuI. Energy dispersive spectroscopy (EDS) on single crystals imaged in the scanning electron microscope (SEM) indicated the presence of Cu, P, As, and I,[15] thus implying that the compound is a quaternary phase. Quantification of As incorporation in crystals of 20%, 35%, 40%, 45%, and 55% As samples was achieved by inductively coupled plasma-mass spectrometry (ICP-MS) and the data are presented in Table 1. In each case, the observed P/As ratio in the product closely mirrors the preparation composition.

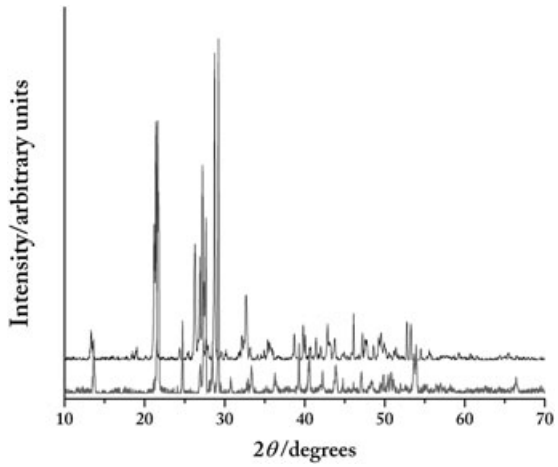

Figure 2. The PXRD patterns of parent (bottom) and 40% As (top) compounds.

The cell parameters of all the compounds were refined from PXRD patterns by using Si as an internal standard (Table 2). The lattice parameters obtained are nearly identical to those found by single-crystal studies for both $(CuI)_8P_{9.6}As_{2.4}$ (20% As, Table 3) and $(CuI)_8P_{7.2}As_{4.8}$ (40% As).[10] The shift of the PXRD patterns of the mixed pnicogen phases towards higher *d* spacing relative to the parent compound (Figure 2) is consistent with an increase in unit cell dimensions upon the substitution of phosphorus with the larger arsenic atoms (Table 2). Together with the narrow peak widths observed in XRD, these data suggest that the compositions can be reproducibly targeted, and there is a narrow phase dispersion among crystals obtained from a single reaction.

Structure analysis for $(CuI)_8P_{9.6}As_{2.4}$: In order to address trends in pnicogen and copper distributions as a function of As incorporation, a single crystal corresponding to 20% As was selected for analysis (Table 3). The 20% As compound (Figure 3) is isostructural to the parent phase, as well as the previously determined 40% As compound,[2,10] and contains eight Cu, eight I, and twelve pnicogen atoms in its asymmetric unit. While the eight I positions are fully occupied, the copper sublattice consists of multiple partially occupied sites. Thus, within a unit cell, the 32 Cu atoms are distributed over 72 identified Cu positions, in contrast to 60 positions reported for $(CuI)_8P_{12}$, and 92 positions reported for $(CuI)_8P_{7.2}As_{4.8}$ (Table 4). Similar to what was observed in the 40% As structure, all the pnicogen positions are shared by P and As, with the highest proportions of As in the "roof" P7 and P10 positions, suggesting clear site preferences for As in the mixed pnicogen chains (Tables 4 and 5). The degree of As occupation is also reflected in the P/As–P/As bond lengths, with longer distances observed for higher average occupancies, similar to what was found for 40% As:[10] P/As7–10 = 2.479(4) Å (average As occu-

Table 3. Crystal data and structure refinement parameters for $(CuI)_8P_{9.6}As_{2.4}$.

formula	$(CuI)_8P_{8.7}As_{3.3}$
M_r	510.12 g
radiation	$Mo_{K\alpha}$
λ [Å]	0.71073
crystal system	monoclinic
space group	$P2_1/c$
a [Å]	15.309(3)
b [Å]	13.057(3)
c [Å]	15.305(3)
α [°]	90.0
β [°]	115.75(3)
γ [°]	90.0
V [Å^3]	2755.4(10)
Z	16
δ_{calcd} [M gm^{-3}]	4.919
μ [mm^{-1}]	19.669
$F(000)$	3581
crystal size [mm]	$0.14\times0.06\times0.04$
θ range [°]	1.48–28.5
hkl range	$0\le h\le20$, $-17\le k\le0$, $-20\le l\le18$
absorption correction	semi-empirical
reflections collected	20266
unique reflections	6774
R(int)	0.07
parameters	344
R	0.0659
R_w	0.1852
GOF	1.10
largest peak/hole [e Å^{-3}]	2.676/−1.928

Table 1. ICP-MS results obtained for different P/As mixed phases.

Target compound	Cu ICP-MS [ppm]	P ICP-MS [ppm]	As ICP-MS [ppm]	Formula based on P,As analyses
$(CuI)_8P_{9.6}As_{2.4}$ (20% As)	35.5(35)	20.0(20)	13.8(14)	$(Cu_{1.01}I)_8P_{9.36}As_{2.64}$[a]
$(CuI)_8P_{7.8}As_{4.2}$ (35% As)	ND	31.0(30)	35.0(30)	$(CuI)_8P_{8.16}As_{3.84}$
$(CuI)_8P_{7.2}As_{4.8}$ (40% As)	43.0(40)	19.0(20)	32.0(30)	$(Cu_{0.98}I)_8P_{7.08}As_{4.92}$[a]
$(CuI)_8P_{6.6}As_{5.4}$ (45% As)	ND	19.0(20)	39.0(40)	$(CuI)_8P_{6.49}As_{5.51}$
$(CuI)_8P_{5.4}As_{6.6}$ (55% As)	ND	13.1(13)	39.4(40)	$(CuI)_8P_{5.36}As_{6.64}$

[a] Cu content was experimentally determined only for 20% and 40% As samples. ND = not determined.

Table 2. Unit cell parameters[a] and cell volumes of mixed pnicogen compounds.

Compound	a [Å]	b [Å]	c [Å]	β [°]	V [Å^3]
$(CuI)_8P_{9.6}As_{2.4}$ (20% As)	15.314(6)	13.062(3)	15.300(8)	115.76(2)	2756.4
$(CuI)_8P_{7.8}As_{4.2}$ (35% As)	15.435(4)	13.201(2)	15.405(5)	115.44(1)	2834.4
$(CuI)_8P_{7.2}As_{4.8}$ (40% As)	15.466(7)	13.205(2)	15.420(7)	115.39(3)	2845.1
$(CuI)_8P_{6.6}As_{5.4}$ (45% As)	15.468(7)	13.222(5)	15.417(9)	115.40(3)	2848.2
$(CuI)_8P_{5.4}As_{6.6}$ (55% As)	15.525(9)	13.214(3)	15.454(9)	115.46(4)	2862.5

[a] Cell parameters obtained from PXRD refinement with an internal silicon standard.

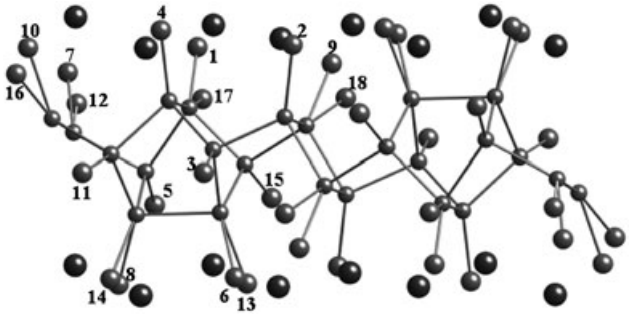

Figure 3. A portion of the crystal structure of $(CuI)_8P_{9.6}As_{2.4}$ with the numbered copper sites bound to the P/As mixed polymer. The dark nonbonded atoms represent the iodine atoms closest to copper. Some of the iodine atoms have been omitted to permit visualization of all copper sites. More detailed illustrations of the parent structure can be found in references [1,2].

Table 4. Comparison of selected structural properties of $(CuI)_8P_{12}$, 20% As, and 40% As compounds.

Structural property	$(CuI)_8P_{12}$ (parent)	$(CuI)_8P_{9.6}As_{2.4}$ (20% As)	$(CuI)_8P_{7.2}As_{4.8}$ (40% As)[10]
no. of Cu positions in unit cell	60	72	92
range of Cu occupancies	0.15(1)-0.97(1)	0.040(10)-0.842(11)	0.057(14)-0.778(13)
As occupancies at 7 and 10	NA[a]	0.617(9)/0.444(8)	0.736(11)/0.647(11)
bond length at P/As7–10 [Å]	2.306(8)	2.478(4)	2.524(4)
range of Cu–Pn distances [Å]	2.17(2)-2.32(2)	2.049(6)-2.317(9)	2.031(7)-2.341(17)

[a] NA = Not applicable.

Table 5. Site occupancy factors (SOFs)[a] for P/As and Cu atoms of $(CuI)_8P_{9.6}As_2$.

Atom	Occupancy	Atom	Occupancy
P/As1	0.83/0.173(10)	P/As7	0.38/0.616(10)
P/As2	0.75/0.253(10)	P/As8	0.71/0.287(11)
P/As3	0.93/0.072(10)	P/As9	0.81/0.194(9)
P/As4	0.75/0.247(10)	P/As10	0.56/0.444(11)
P/As5	0.79/0.202(10)	P/As11	0.68/0.318(10)
P/As6	0.83/0.166(10)	P/As12	0.67/0.327(11)
Cu1	0.781(11)	Cu10	0.644(12)
Cu2	0.467(14)	Cu11	0.818(13)
Cu3	0.567(12)	Cu12	0.628(12)
Cu4	0.621(11)	Cu13	0.338(12)
Cu5	0.164(14)	Cu14	0.195(17)
Cu6	0.179(13)	Cu15	0.204(16)
Cu7	0.846(12)	Cu16	0.077(15)
Cu8	0.690(13)	Cu17	0.040(10)
Cu9	0.562(11)	Cu18	0.193(16)

[a] The SOF is equal to 1 for a fully occupied position. Iodine sites were fully occupied.

pancy: 0.53), P/As2–3 = 2.203(8) Å (average As occupancy: 0.16). The positions P/As11 and P/As12 in the P_4 planar ring have the next highest occupancy of As within the polymer: 0.318(10) and 0.327(11), respectively. Each P/As atom is bonded to three other neighboring P/As atoms and one or two Cu atoms. In contrast to what was seen in the 40% As structure, there are no Cu positions outside a reasonable bonding distance to the pnicogens and the average Cu–P/As bond lengh is 2.18(7) Å. The Cu atoms are associated with one P/As and three I atoms and adopt a distorted tetrahedral geometry.

Investigating the structure of the polymer chain by solid-state NMR spectroscopy and X-ray powder diffraction: To gain further insight into the local structure within the pnicogen chains, solid-state ^{31}P NMR spectroscopy was utilized. Solid-state ^{31}P magic angle spinning (MAS) NMR experiments conducted upon $(CuI)_8P_{12}$ and $(CuI)_8P_{7.2}As_{4.8}$ at high spinning speeds (ν_{rot} between 26 and 29 kHz) yielded markedly different spectra (Figure 4a and b). The ^{31}P MAS NMR spectrum of $(CuI)_8P_{12}$ (Figure 4a) is almost identical to spectra of $(CuI)_8P_{12}$ recently reported by Eckert and co-workers.[16] Fine structure is observed, indicative of a complex J coupling network between the ^{31}P nuclei. In addition, the fast MAS essentially removes most of the line broadening arising from homonuclear dipolar coupling. This spectrum arises from 12 magnetically distinct ^{31}P nuclei, whose preliminary assignments were made by Eckert et al. using several two-dimensional NMR experiments and quantitative chemical shift comparisons.[16]

The ^{31}P MAS NMR spectrum of $(CuI)_8P_{7.2}As_{4.8}$ (Figure 4b) bears little resemblance to the spectra of $(CuI)_8P_{12}$. The peaks are substantially broadened and shifted, with none of the resonances matching any of those found in spectra of $(CuI)_8P_{12}$, suggesting the local phosphorus environment has changed (Figure 4c, d). There are sharp resonances visible at $\delta = 5.3$ and -14.2 ppm that likely correspond to some sort of impurity phase (indicated by the daggers in Figure 4b), possibly some sort of phosphate or phosphite, which are known to have chemical shifts in this region.[16,17] The broadening and shifting of the ^{31}P resonances is the result of several factors, including 1) indirect spin–spin coupling (J coupling) between ^{31}P and ^{75}As nuclei (^{75}As is a quadrupolar nucleus with a nuclear spin of 3/2); 2) residual dipolar coupling between ^{31}P and ^{75}As nuclei, which cannot be removed by MAS;[18] and 3) scalar relaxation of the second kind of the ^{31}P nucleus (resulting from J coupling to ^{75}As). All three of these factors have been observed to drastically alter ^{31}P powder patterns for spin pairs involving half-integer quadrupolar nuclei, resulting in fine structure, line broadening, and apparent shifts in the centre of gravity of the powder patterns.[19,20] In addition, each phosphorus site will have three nearest neighbours in the first coordination sphere, which may consist of P and As atoms in ratios of 3:0, 2:1, 1:2 and 0:3, with the 2:1 and 1:2 ratios being the most common. This, in combination with additional site variability in the second coordination sphere, means that each phosphorus site will have a broadened resonance resulting from a distribution of chemical shifts.[21] Spin–spin coupling from multiple ^{31}P and/or ^{75}As nuclei further convolute the ^{31}P NMR spectra; however, additional

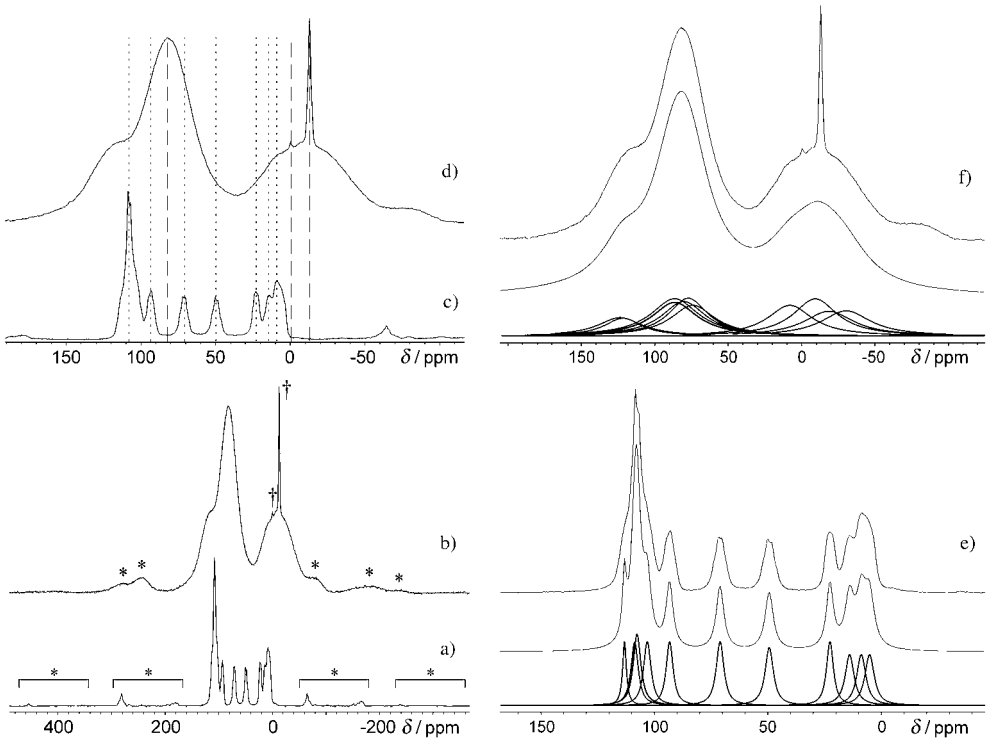

Figure 4. ^{31}P fast MAS NMR spectra of a) $(CuI)_8P_{12}$ ($\nu_{rot}=28$ kHz) and b) $(CuI)_8P_{7.2}As_{4.8}$ ($\nu_{rot}=26$ kHz) acquired at 9.4 T. Asterisks denote spinning sidebands and daggers denote possible impurities. Expanded isotropic region of the ^{31}P MAS NMR spectra of c) $(CuI)_8P_{12}$ and d) $(CuI)_8P_{7.2}As_{4.8}$. Dotted and dashed lines are used for comparison of peak positions in $(CuI)_8P_{12}$ and $(CuI)_8P_{7.2}As_{4.8}$, respectively. Experimental (top), simulated (middle) and deconvoluted (bottom) ^{31}P MAS NMR spectra of e) $(CuI)_8P_{12}$ and f) $(CuI)_8P_{7.2}As_{4.8}$.

coupling from ^{65}Cu can be neglected in this instance, as there is no evidence of dipolar coupling between ^{31}P/^{75}As and copper in these materials (see below) or between ^{65}Cu and ^{31}P in $(CuI)_8P_{12}$.[16]

To obtain a simulation of the ^{31}P MAS NMR spectrum of $(CuI)_8P_{7.2}As_{4.8}$, the assignments of the resonances in $(CuI)_8P_{12}$ should first be considered. In Table 6 a comparison is made between the assignments of Eckert and co-workers, and our assignments, which differ only slightly. From high to low frequency, there are 12 resonances arranged to form six distinct spectral regions, which integrate as 5:1:1:1:1:3 (Figure 4a). The high-frequency ^{31}P resonances are assigned to the sites in the "roof" positions (P7, P10), as well as directly bound sites, P3, P9, P6 and P5 (Figure 1b). Eckert et al. utilized radio frequency driven dipolar recoupling (RFDR) and total through-bond correlation spectroscopy (R-TOBSY) augmented with R30(6)(14) pulse symmetry to assign the resonances at $\delta=71.1$ and 49.4 ppm to P1 and P4, respectively, and the remaining sites are assigned as listed in Table 6. We propose a slightly alternative assignment based on ^{31}P fast MAS correlation spectroscopy with TPPI scheme (tppi-COSY) NMR spectra acquired in our laboratory (Figure 5). The resonances at $\delta=71.1$ and 49.4 ppm are assigned to P2 and P8, respectively, and the terminal P1, P4 and P11, P12 pairs are assigned to the low-frequency shifts as noted in Table 6. Cross peaks indicating direct connectivity are observed for most directly bound phosphorus pairs;

Table 6. Assignments of phosphorus sites for ^{31}P MAS NMR spectra of $(CuI)_8P_{12}$ and $(CuI)_8P_{7.2}As_{4.8}$.

$(CuI)_8P_{12}$ P site assignments		
ref. [16]	This work	δ_{iso} [ppm]
P3, P9, P7,	P9	113.2
P10, P6	P7	108.7
	P10	108.7
	P3	107.7
	P6	103.2
P5	P5	93.3
P1	P2	71.1
P4	P8	49.4
P2	P12	22.7
P11	P4	14.0
P8	P1	8.9
P12	P11	5.2

$(CuI)_8P_{7.2}As_{4.8}$ P site assignments		
This work	δ_{iso} [ppm]	FWHH [Hz]
P7, P10	122	5000
	117	5000
P3, P9,	87	5000
P5, P6,	84	5500
P2, P8	82	5000
	80	5500
	80	5250
	76	6000
P1, P4,	10	6000
P11, P12	−4	5000
	−18	5000
	30	6000

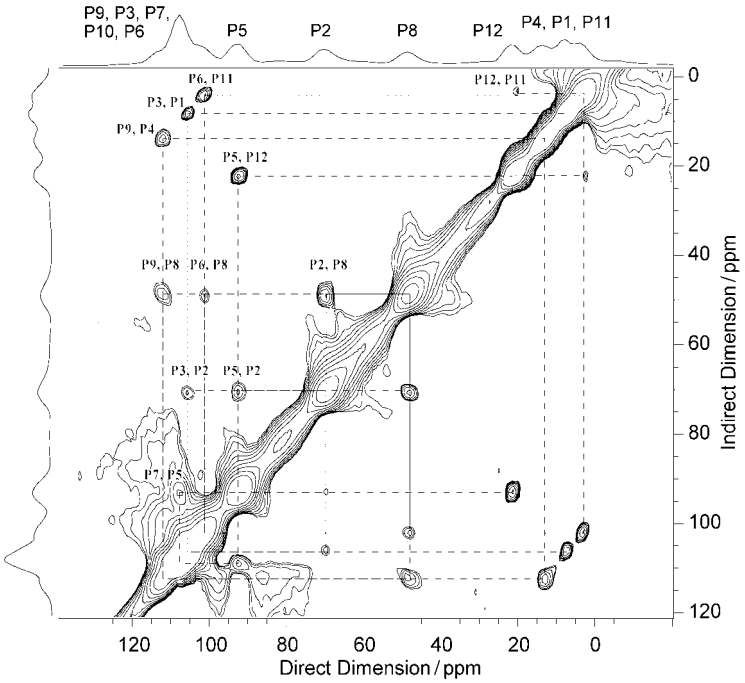

Figure 5. ^{31}P tppi-COSY MAS NMR spectrum of $(CuI)_8P_{12}$ acquired with $\nu_{rot}=27$ kHz. The vertical spectral scale is ca. 0.9–1.0% of the maximum height, processed with complete phasing of the direct and indirect dimensions.

however, cross peaks are not observed between P7 and P10, due to overlap with diagonal peaks. In addition, intense cross peaks do not result from couplings between P11 and P12, or P1 and P4, possibly due to the different nature of the spin systems at these sites (e.g., P1 is coupled to two P4 nuclei and one P3 nucleus). A simulated one-dimensional spectrum based on these assignments is presented as the middle trace of Figure 4e. Only chemical shifts are taken into account, while fine structure resulting from *J* coupling is neglected, though roughly accounted for by peak broadening on the order of 500 to 700 Hz at full-width-at-half-height (FWHH). Complex spin-system analysis is prohibited by overlapping peaks and broadened resonances.

Based on our assignments for $(CuI)_8P_{12}$, the ^{31}P fast MAS NMR spectra of $(CuI)_8P_{7.2}As_{4.8}$ are simulated by using the following assumptions:

1) Fine structure resulting from *J* coupling and residual dipolar coupling will not be observed, due to both rapid scalar relaxation of the second kind at the phosphorus nucleus and spin–spin coupling from multiple sites. As a result, individual spin–spin interactions are not considered.
2) Chemical shift dispersions result from variable substitution of P and As sites in the first and second coordination spheres, serving to further broaden the individual resonances.

To approximate these effects, peaks with FWHH ranging from 5000 to 6000 Hz are utilized. The relative integrated areas of the peaks utilized in the simulations are obtained from the site occupancies reported previously.[10] Aside from broadening of peak widths and chemical shift distributions, the average ^{31}P chemical shifts change due to As substitution. In Figure 6a, the simulation uses the same chemical shifts as found in the ^{31}P NMR spectra of $(CuI)_8P_{12}$, and the appropriate site weightings, producing a spectrum that is completely different from the experimental spectrum. In Figure 6b, new chemical shift assignments are made for all twelve sites, but the sites are unweighted (equal integrated intensities), amounting to three major spectral regions with integrated intensities of 2:6:4 from high to low frequency. This simulated spectrum resembles the experimental data, but further agreement can be obtained by using the appropriate phosphorus-site weightings determined from single-crystal X-ray diffraction (Figure 6c).[10] A full listing of assignments is shown in Table 6 and detailed simulations

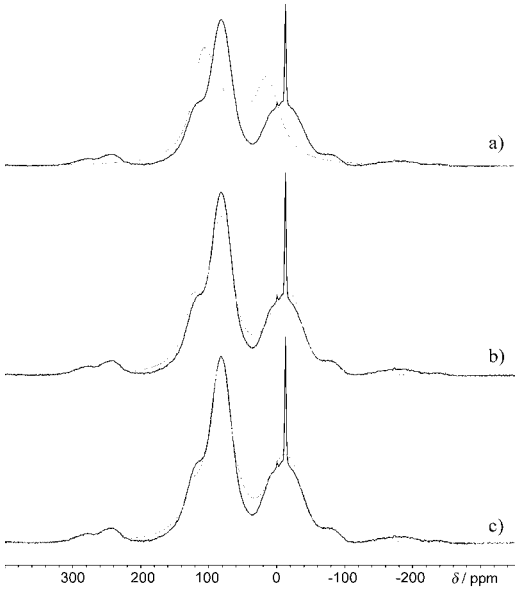

Figure 6. Experimental (black, solid) and simulated (gray, dashed) ^{31}P MAS NMR spectra of $(CuI)_8P_{7.2}As_{4.8}$: a) simulation using the same chemical shifts as $(CuI)_8P_{12}$; b) simulation using modified chemical shifts and equal peak intensities; c) simulation using modified chemical shifts and weighted peak intensities. Chemical shifts are listed in Table 6, weightings are described in ref. [10].

showing spectral contributions from individual sites are shown in Figure 4f.

A true solid solution[22] (random distribution) would result in a linear relationship of unit cell volume with respect to the amount of As, consistent with the three-dimensional interpretation of Vegard's Law.[23,24] A graph of unit cell volume versus percentage of As is presented in Figure 7.

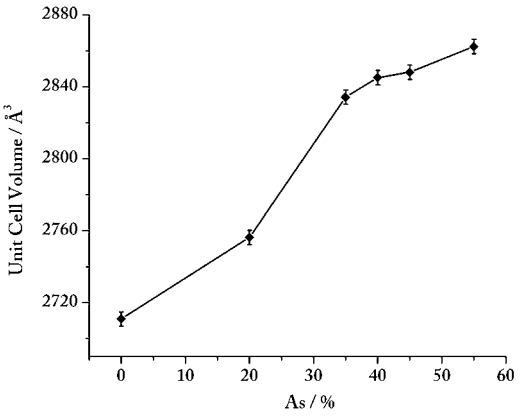

Figure 7. Plot of unit cell volume as a function of arsenic content for $(CuI)_8P_{12-x}As_x$, in which $x = 0$, 2.4, 4.2, 4.8, 5.4, and 6.6.

Overall, the correlation is nonlinear, with a rapid increase in cell volume from the parent to 35% As, followed by a gradual increase from 35% to 55% As. The lack of linearity (i.e., deviation from Vegard's Law) is fully consistent with the preferred site occupation of As in the pnicogen chains noted in the single-crystal studies for the 20 and 40% structures. The ^{31}P NMR data are not inconsistent with this analysis. Although the resolution of the ^{31}P NMR spectra for the 40% As mixed pnicogen compound is poor due the large distribution of chemical shifts, relaxation, and spin–spin coupling effects, the simulation based upon the X-ray single-crystal model does show a marginally better fit than that obtained by a random distribution of As throughout the chain.

Hönle and von Schnering and have likewise reported site preferences for arsenic in some polypnicogen phases. For Hittorf's modification of phosphorus (Figure 1a) they found that about 5% As can be adopted into the structure, and the As is situated uniquely at one of the two equivalent "roof" sites in the [P8] cage.[25] The selective site occupation was attributed to a release in strain within the polymer, predicted by modeling. Indeed, crystallization of Hittorf's phosphorus was reported to be easier in the presence of As, consistent with increased stability of the mixed pnicogen phase.[25] As indicated here, we also see strong site preference for the "roof" positions within the analogous [Pn8] cages of $(CuI)_8P_{12-x}As_x$, although we are able to substitute far more As into this structure than is reported for Hittorf's phosphorus. Likewise, we find that crystal growth is more facile (as evidenced by the number and size of crystals achieved in the transport reactions) when As is included in the reaction. Thus, our results are consistent with the strain arguments postulated by von Schnering. However, a more recent and detailed theoretical analysis by Böcker and Häser indicates that the structure of Hittorf's phosphorus is essentially strain free.[11] Among the small clusters calculated for the formula P_8, the highly symmetric fused 5-ring structure P8(0) is the lowest in energy.[11] Additionally, Baudler, has reported a number of molecular analogues that feature the P8(0) unit in question, arguing against significant strain.[26] The origin of the preferred site occupation remains unclear, but may be due to subtle bonding preferences. We speculate that the extent of transport growth may be a function of differences in the volatilization/condensation of the precursors and products upon As incorporation, as described below.

Influence of As on thermal stability: To gain some insight into the decomposition mechanism, stability, and volatility of the products, thermal gravimetric analyses (TGA) were conducted under a dynamic atmosphere of N_2 from ambient temperature to 800°C. For the 40% As compound, an initial weight loss was observed at 439°C (Table 7), which levels off significantly around 475°C, corresponding to a loss of about 30%. PXRD patterns of $(CuI)_8P_{7.2}As_{4.8}$ heated in a flow furnace at 450°C under an inert atmosphere revealed the presence of a combination of CuI and unreacted mixed pnicogen phase. This suggests that this first weight loss is likely due to decomposition of $(CuI)_8P_{7.2}As_{4.8}$ to CuI and volatile P/As; that is, under flow conditions in an open system decomposition begins at approximately 440°C. The predicted weight loss for the 40% As phase losing volatile pnicogen is 27.7%, very close to what we see (~30%). Subsequent weight losses are observed up to about 750°C, at which point ~90% of the initial weight has been lost. The PXRD pattern taken on a sample heated up to 800°C shows CuI as the only product. Since CuI melts near 600°C, the latter weight loss is attributed to volatilization of CuI (which may be incomplete, due to the timescale of the study). Therefore, we presume that the pnicogens are lost first, followed by the volatilization of CuI, although these processes may be competitive with volatilization of the quaternary phase. There is no systematic relationship between the decomposition temperature (first weight loss onset) and the composition (Table 7); however, all of the mixed pnicogen phases demonstrate higher decomposition temperatures than the pure phosphorus parent compound.

Table 7. The temperatures of initial weight loss (onset) for parent and mixed pnicogen compounds.

Compound	T (decomp) [°C]
$(CuI)_8P_{12}$	342
$(CuI)_8P_{9.6}As_{2.4}$ (20% As)	405
$(CuI)_8P_{7.8}As_{4.2}$ (35% As)	406
$(CuI)_8P_{7.2}As_{4.8}$ (40% As)	439
$(CuI)_8P_{6.6}As_{5.4}$ (45% As)	402
$(CuI)_8P_{5.4}As_{6.6}$ (55% As)	417

From these analyses, it is not clear if the "roof" position preference of As has any contribution to the thermal stability of these materials relative to the parent compound. Since the decomposition products are necessarily different in each case, and have unknown enthalpies, the relative energies of the various phases cannot be quantitatively assessed. However, we note that an apparent lower volatility of the products that incorporate As (which could be predicted based on formula weight alone) is consistent with the growth of more/larger crystals for these phases relative to the all-phosphorus phase.

Copper disorder and ionic conductivity: The trend in copper disorder in these phases can be ascertained by evaluation of the number of copper positions in the single-crystal structures (Table 4). Among the 18 Cu positions in the asymmetric unit of the 20% As compound, 15 positions can be exactly matched with the parent compound. On the other hand, all the 18 positions in the 20% As structure can be found in the 40% As compound, although there are an additional five copper positions. These five copper positions have considerably longer bond lengths to the pnicogen chains (2.83(7) to 2.99(8) Å, relative to 2.03–2.34 Å for the other Cu–Pn distances in the structure) and represent ~7% of the copper in the structure.[10] The increased number of copper positions suggests a decreased thermodynamic site preference, whereas the presence of copper sites outside a normal bond length to the pnicogen chain suggests weaker Cu–Pn interactions. Hence, increasing Cu^I ion conductivity may be anticipated with increasing As incorporation.

The ^{65}Cu MAS NMR spectrum of $(CuI)_8P_{7.2}As_{4.8}$ consists of a large isotropic peak centered at $\delta = -3$ ppm flanked by spinning sidebands, and a low intensity side peak at $\delta = -21$ ppm (Figure 8). Fixed Cu positions result in ^{65}Cu NMR spectra with distinct second-order line shapes, and have further effects on the ^{31}P MAS NMR spectra;[27] however the peak at $\delta = -3$ ppm has a FWHH of about 1300 Hz and exhibits no second-order quadrupolar line shape, which is consistent with the fast ionic motion of the Cu^I ions in this compound. Similar ^{65}Cu NMR spectra have been measured for $(CuI)_8P_{12}$, in which the Cu^I ions are also mobile.[16] It is not possible to evaluate the relative conductivities by this technique without performing temperature-dependent studies. Therefore, impedance spectroscopy was utilized to quantify the effect of As incorporation on the ionic conductivity in these compounds.

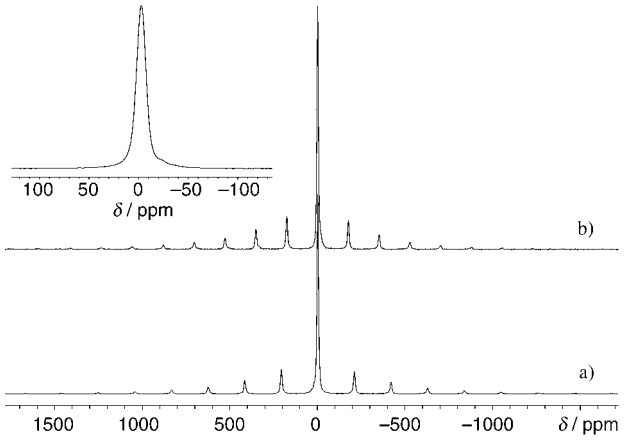

Figure 8. ^{65}Cu MAS NMR spectra collected at 9.4 T at spinning speeds of a) 23 kHz and b) 20 kHz. The inset shows an expansion of the isotropic central transition.

The complex plane plots (Nyquist plots) of 35% As, 45% As, and $(CuI)_8P_{12}$ polycrystalline pellet samples (30°C) are presented in Figure 9. The inclined spike (Warburg element) arising at low frequency is attributed to charge build up at the blocking electrode, and is characteristic of an ionic conducting material (ions cannot pass through the sample–electrode interface). The high-frequency arcs consist of two overlapping arcs of similar capacitance attributed to bulk (or intragranular), and grain-boundary (or intergranular) regions of the sample. These regions are responsible for the intrinsic (σ_b) and grain-boundary (σ_{gb}) conductivity, respectively; the total conductivity (σ_t) is calculated from the intersection of the Warburg element with the low-frequency arc at the real axis. In contrast, the bulk and grain-boundary contributions in $(CuI)_8P_{12}$ are resolved as two discernable arcs with capacitances that differ by five orders of magnitude (Figure 9). The disparity in capacitance values for the grain-boundary contributions can be attributed to the relative polarizabilities of P and As. The lower polarizability of P in the parent compound results in a greater degree of charge accumulation at the grain boundaries upon application of a potential field, and thus $(CuI)_8P_{12}$ has a higher grain-boundary capacitance. In contrast, the more polarizable As results in electronically leaky grain boundaries with decreased capacitive behavior.[28–30]

According to the impedance data at 30°C, the bulk and the total conductivities of all the samples are of the same order of magnitude, regardless of As content (Figure 9). The total conductivity at 30°C for the parent material, extracted from the literature,[8] is estimated to be $1.5\times10^{-6}\,S\,cm^{-1}$, which is smaller than the value of $5.1\times10^{-6}\,S\,cm^{-1}$ obtained in this work. This difference is likely an effect of disparities in the grain-boundary structure from sample to sample. Additionally, variable-temperature measurements on a 40% As sample (Supporting Information) revealed Arrhenius-type behavior and calculated activation energies of 0.44 eV and 0.40 eV for bulk and grain-boundary conductivities, respectively, similar to the corresponding activation energy reported for $(CuI)_8P_{12}$ (0.45 eV).[8]

Although the bulk values (σ_b) obtained here might be considered to be an intrinsic measure of the material conductivity, preferred orientation effects are likely to have a profound influence on the copper ion conductive pathways. It has been established from single-crystal studies on $(CuI)_8P_{12}$ that the ionic conducting pathway is along the axis of the pnicogen chains, which coincides with the long axis of the needle crystals.[8] In pressed pellets, these needles are likely to be oriented perpendicular to the electrodes, due to gravitational settling and applied pressure, resulting in

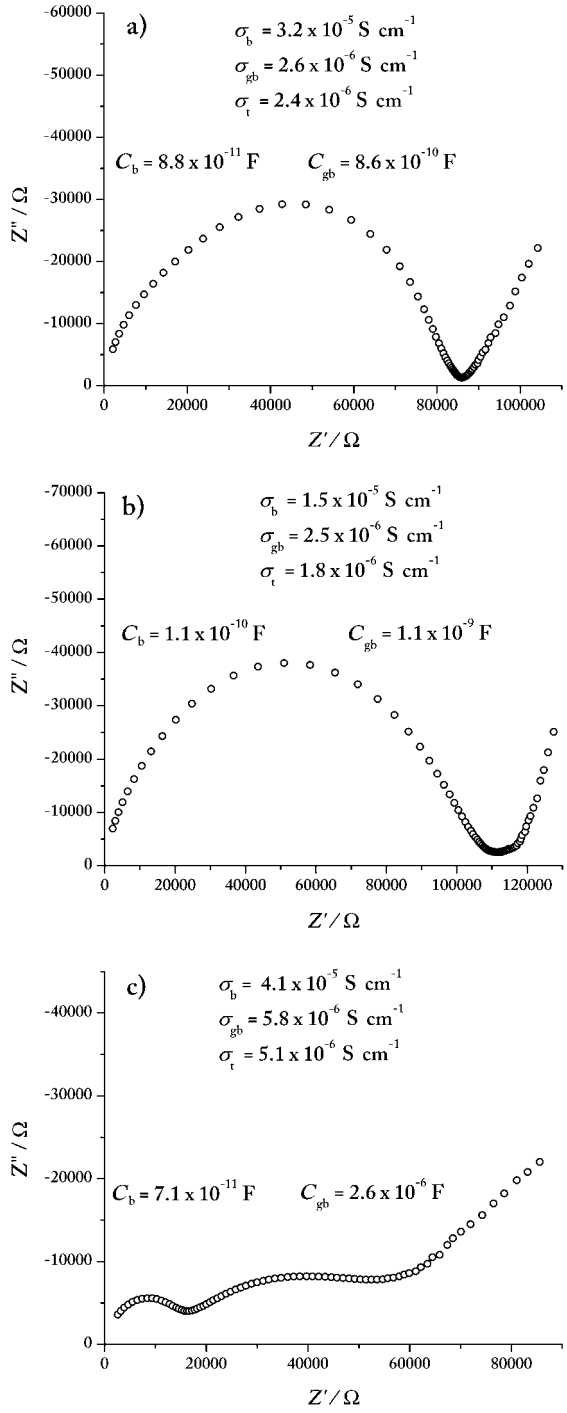

Figure 9. The complex plane impedance plots of a) 35% As, b) 45% As, and c) $(CuI)_8P_{12}$ polycrystalline pellet samples at 30°C.

values that are not representative of the optimal conductivities. Indeed, a decrease in conductivity of about 30% is observed in polycrystalline samples of $(CuI)_8P_{12}$ relative to single crystals measured along the needle axis.[8] Hence, no definitive conclusions about the relative differences in conductivity as a function of As incorporation can be made based on polycrystalline samples. Accordingly, a single-crystal impedance spectroscopy study on the 40% mixed pnicogen phase has been performed to assess the conductivity along the needle axis and provide a meaningful comparison to $(CuI)_8P_{12}$.

An impedance plane plot for a single crystal of $(CuI)_8P_{7.2}As_{4.8}$ (40% As) at 128°C with the electrodes applied perpendicular to the needle axis is shown in Figure 10.

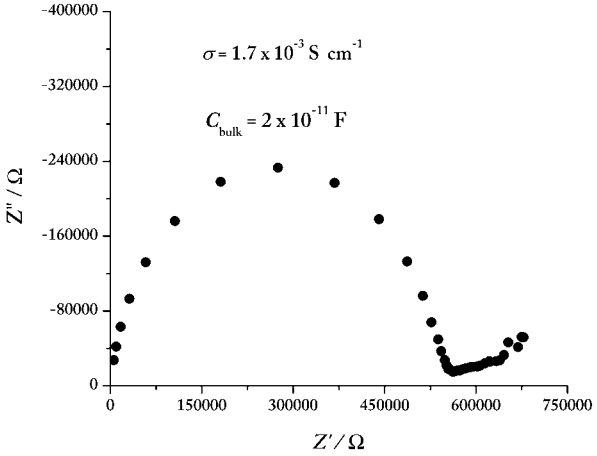

Figure 10. The complex plane plot of a single crystal of $(CuI)_8P_{7.2}As_{4.8}$ (40% As) at 128°C.

An almost semicircular response, corresponding to bulk sample, is prominent. A remarkably high conductivity of 1.7×10^{-3} S cm^{-1} is obtained along the needle axis, comparable to values obtained for single crystals of $(CuI)_8P_{12}$ at much higher temperatures (1.9×10^{-3} S cm^{-1} at 186°C),[8] and roughly an order of magnitude greater than the single-crystal conductivity for $(CuI)_8P_{12}$ at similar temperatures (ca. 3×10^{-4} S cm^{-1} at 130°C, estimated from an Arrhenius plot, reference [8]). This suggests a significant improvement in conductivity, at least along the needle axis, upon As incorporation. The influence of preferred orientation effects in polycrystalline pellets is evident in the corresponding bulk conductivity value obtained for a polycrystalline 40% As sample at 124°C, 8.4×10^{-4} S cm^{-1}.

Conclusion

In an exploration of heavier pnicogen analogues of $(CuI)_8P_{12}$, we were successful in synthesizing a series of neutral P/As mixed pnicogen analogues with As incorporation of up to 55%. These phases are isostructural to $(CuI)_8P_{12}$, as evidenced by X-ray crystallography and ^{31}P solid-state NMR spectroscopy, and X-ray diffraction studies further indicate that the arsenic has a strong site preference for the "roof" positions in the pnicogen polymer. The As substitution in $(CuI)_8P_{12}$ results in an increase in the thermal degradation temperature for the material, and an increase in copper-ion disorder. The latter is manifested as an increased conductivity in $(CuI)_8P_{7.2}As_{4.8}$ (40% As) relative to $(CuI)_8P_{12}$, when measured along the needle axis of single crystals. However,

in polycrystalline samples, very little conductivity difference is observed as a function of As content, ascribed to a more convoluted pathway for conduction that arises from crystallite orientation effects within the pressed pellets.

Experimental Section

Solid-state synthesis: The mixed pnicogen compounds $(CuI)_8P_{12-x}As_x$, in which $x=2.4$, 4.2, 4.8, 5.4, and 6.6, were synthesized from stoichiometric combinations of CuI (Aldrich 99.999%), red P (Strem 99%), and powdered As (Alfa Aesar 99.999%). The reagents were ground together, pressed into a pellet, and heated at 550°C for two weeks in evacuated fused-silica tubes of 13 mm inner diameter and about 80 mm length. The sample pellets were kept at the hot end of the ampoule, nearest to the thermocouple, to facilitate transport of crystals to the cool end. For reactions that produced only small amounts of transported crystals, the products (pellet and crystals) were reground and reheated for an additional two weeks in order to produce a second batch of crystals (recrystallization). All analyses on powders were performed on ground single crystals. In cases in which CuI was observed (as a white deposit) on the crystals under the light microscope, the crystals were sonicated in CH_3CN first to wash away impurities. Likewise, if the presence of CuI was detected by PXRD in ground samples, the powdered sample was stirred in CH_3CN overnight to dissolve CuI. Overall yields (based on powder X-ray diffraction) ranged from 80–100%. Yields of crystals were high when large As concentrations were employed (up to 75% of the sample as crystals for 40% As inclusion) and lower for small concentrations (less than 25% of the sample as crystals for 20% As inclusion).

X-ray single-crystal structure analysis: A single-crystal structure analysis was performed on a sample prepared from a 20% As, 80% P reaction (Table 2). A single crystal of dimensions $0.14\times0.06\times0.04\,mm^3$ was mounted on a piece of glass fiber with epoxy resin, and data were collected from a Bruker P4/CCD single-crystal diffractometer with $Mo_{K\alpha}$ radiation ($\lambda=0.71073$ Å). The structure solution and refinement were performed using the SHELXTL package of crystallographic programs (Bruker Analytical, Inc.).

The structure solution software recommended a tetragonal or orthorhombic unit cell; however, since twinning similar to that observed in $(CuI)_8P_{12}$ was suspected[2] the lower symmetry monoclinic option ($P2_1/c$) was chosen. The function TWIN was used in the structure refinement to account for *a*/*c* exchange due to twinning. The structure modeling for the 20% As compound was performed as follows: from the difference map eight I atoms were found in similar positions to those reported for the parent compound (most intense set of peaks). Since a careful analysis of the frames data (30 s per frame) revealed no suggestion of superstructure, P and As were presumed to be occupying the same sites. The next set of peaks with appreciable electron density were assigned to P and As as shared occupancies summing to 1.0. The percent occupancies of As refined to 27.5% instead of the expected 20%, but fixing of the sum of occupancies to equal 20% did not result in a substantial change in the *R* value; however, some of the displacement parameters were poorly behaved. The As occupancy was left unconstrained in the final solution.

The remaining peaks found to be within reasonable bond lengths to P/As and/or I were assigned to Cu sites ranging from a 4 (minimum) to 85% occupation. After assignment of 18 independent Cu positions, attempts to satisfy remaining peaks in the difference map with partially occupied copper sites resulted in sites that were too close to P/As positions to be real and were thus discarded. Without restraint, the Cu occupancies sum to 7.41 (i.e., 1.85 Cu atoms out of 2.0 expected). These occupancies were constrained to sum to 8.0 (consistent with the concentration of copper obtained by elemental analysis, Table 1) without any significant change in *R* value. When all the atoms (Cu, P, As, I) were allowed to refine anisotropically, reasonable values were obtained for all positions except Cu7, Cu8, Cu10, Cu16, Cu17, and Cu18. Hence, these were left isotropic. The occupancy of the Cu17 position was difficult to refine freely and therefore was fixed to a reasonable occupancy value. The structure refined with 37.7% twinning to an *R* value of 6.59%. Further details of the crystal structure investigation can be obtained from the Fachinformationszentrum Karlsruhe, 76344 Eggenstein-Leopoldshafen, Germany, (fax: (+49)7247–808–666; e-mail: crysdata@fiz.karlsruhe.de) on quoting the depository number CSD-414237.

Powder X-ray diffraction (PXRD): Products consisting of transported material and the remaining residue of the pellets from each reaction were separated and ground to carry out PXRD studies. A Rigaku D Max RU 200B instrument with voltage and current of 40 kV and 100 mA, respectively, was used to collect PXRD patterns. The powdered samples were dusted onto double-sided sticky tape attached to an aluminum holder, or a thin layer of petroleum wax coated on a quartz (0001) low background holder. Unit cell refinement was performed on data collected from long scans (ca. 1.5 h) referenced to an internal silicon standard. The peaks were refined with the program CELREF V3 using least-squares methods and discarding only peaks of $<3\%$ relative intensity.

Inductively coupled plasma-mass spectrometry analysis (ICP-MS): Samples for chemical analyses were prepared by dissolving about 20 mg of the powdered crystals in 10–15 mL of conc. HNO_3 and diluting to 100.0 mL with distilled water in a volumetric flask. P and As ratios were determined for all the samples, and Cu amounts were determined for the 20% and 40% As samples (Table 1) on which single-crystal studies were performed.

Solid-state NMR spectroscopy: Solid-state ^{31}P and ^{65}Cu MAS NMR experiments were conducted on $(CuI)_8P_{12}$ and $(CuI)_8P_{7.2}As_{4.8}$ using a Varian Infinity Plus 9.4 T NMR spectrometer operating at $\nu_0(^{31}P)=161.8$ MHz and $\nu_0(^{65}Cu)=113.5$ MHz. Varian/Chemagnetics 2.5 mm HX MAS and 4 mm HXY triple-resonance probes were used. All samples were ground into fine powders and tightly packed into 2.5 mm and 4 mm o.d. zirconium oxide rotors. Spectra were acquired using both a conventional Bloch decay pulse sequence and a rotor-synchronized Hahn-echo pulse sequence of the form $[(\pi/2)_x\text{-}\tau_1\text{-}(\pi)_y\text{-}\tau_2\text{-acquire}]$. Phosphorus chemical shifts were referenced to 85% H_3PO_4 with $\delta_{iso}(^{31}P)=0$ ppm. Relevant acquisition parameters include a 90° pulse width of 1.6 μs ($\nu_1=160$ kHz) and calibrated recycle times of 15 s. Samples were spun between 17 kHz and 26 kHz and from 768 to 1600 transients were collected per experiment. ^{31}P-^{75}As transfer of populations in double resonance (TRAPDOR) NMR experiments[31] utilized an rf field of about 72 kHz on the ^{75}As channel, but were unsuccessful in indirectly resolving the ^{75}As quadrupolar coupling constants (likely due to very large ^{75}As quadrupolar coupling constants and inconvenient relaxation characteristics). Copper chemical shifts were referenced to solid CuCl ($\delta_{iso}(^{65}Cu)=0$ ppm). For rotor-synchronized ^{65}Cu MAS NMR experiments, the central-transition selective 90° pulse width was 2.0 μs (with $\nu_1(^{65}Cu)=125$ kHz) and the calibrated recycle time was 0.2 s. Samples were spun at 20.0 kHz and 23.7 kHz and the number of transients collected ranged from 32000 to 220000.

Two-dimensional ^{31}P NMR experiments were conducted upon $(CuI)_8P_{12}$ employing the conventional COSY pulse sequence, as well as the tppi-COSY sequence.[32] The 2.5 HX fast MAS probe was used for these experiments, with the sample spun at 27 kHz. The 90° pulse width was set to 1.40 and 1.95 μs for COSY and tppi-COSY NMR experiments, respectively. Spectral widths in the COSY and tppi-COSY were 100 kHz and 200 kHz, respectively. 32 (COSY) and 16 (tppi-COSY) transients were collected for the direct dimension, and 256 and 512 increments were collected for the indirect dimension.

Spectra were simulated by using the line-fitting routine in the NUTS software package (Acorn NMR). A simplex routine was used to accurately fit the spectra, allowing flexibility in the frequency, line width, and Lorentzian/Gaussian character, while keeping the, a priori, integrated intensity of the peaks constant.

Thermogravimetric analysis: Thermogravimetric analyses were performed on a Pyris 1 TGA instrument. Samples were analyzed in ceramic pans at a heating rate of $2\,°C\,min^{-1}$ to 500°C and $10\,°C\,min^{-1}$ from 500–800°C in a dynamic N_2 atmosphere. The open-system ensures that volatilization of products will drive equilibria forward, and is therefore not representative of thermal treatments conducted in sealed ampoules. The slow initial rate was employed to quantify the onset for the first weight loss and this was used to assign the relative stability of the compounds to

thermal decomposition. The small quantity of residue that was obtained from the 40% As sample after being heated to 800°C, was analyzed by powder X-ray diffraction. To determine the products after the first weight loss, X-ray diffraction data were acquired on a 40% As sample previously heated to 450°C under a flow of argon.

Conductivity measurements: The ionic conductivity properties for polycrystalline samples of the parent, and the 35% As, 40% As, and 45% As phases were studied using impedance spectroscopy (IS). Polycrystalline samples of 35% As, 45% As, and $(CuI)_8P_{12}$ were sieved in order to produce uniform grain sizes, thereby permitting reasonable comparison of data from different preparations. The samples were made by cold pressing the powdered material in a 0.625 cm die with an applied pressure of about 4.5 metric tons. The exact thickness of the pellets was measured with a Vernier micrometer (all were = 1 mm). Opposite sides of the pellets were sputter coated with gold electrodes and each pellet was then loaded into a pressure cell with flat Ni electrodes on both sides. The sample was placed in an oven and was continuously flushed with argon gas during the measurements in order to avoid oxidation of the samples.

The sample for single-crystal impedance measurements was prepared by embedding a long (ca. 4 mm) needle crystal in an epoxy matrix, allowing the epoxy resin to harden, and cutting it into a pellet of about 1.5 mm thickness with exposed crystal faces. The cross-sectional area of the crystal faces was measured and then sputter coated with gold electrodes. The impedance measurements were conducted as described for the polycrystalline sample.

A Solartron 1260 Impedance/Gain-Phase Analyzer was used to take the IS measurements at an applied voltage of 100 mV and a frequency range of 30 mHz to 1 MHz. For the sieved polycrystalline samples of 35% As, 45% As, and $(CuI)_8P_{12}$ the impedance data were acquired at 30°C. Variable-temperature IS measurements were taken for a nonsieved polycrystalline sample of 40% As in the temperature range 30 to 124°C. Single-crystal studies of the 40% As sample were conducted only above 120°C, as the small cross-sectional area of the needles resulted in resistance values outside the range of the instrument at lower temperatures. The complex impedance curves were analyzed using the ZView program to determine the corresponding equivalent circuits and compute the bulk and grain-boundary conductivities.

Acknowledgements

B.J. and S.L.B. acknowledge Research Corporation (Research Innovation Award, R10617), Wayne State University-Institute of Manufacturing Research, and NSF-CAREER (DMR-0094273) for financial support of this work. R.W.S. and A.Y.H.L. acknowledge the Natural Sciences and Engineering Research Council (NSERC, Canada) for research support, and the Canadian Foundation for Innovation (CFI), Ontario Innovation Trust (OIT) and the University of Windsor for funding the solid-state NMR laboratories. We thank Prof. Jen Aitken at Duquesne University and Dr. Mary Jane Heeg at Wayne State University for assistance with X-ray structural analyses and Dr. Ion Halalay at GM R&D for assistance with impedance spectroscopy measurements and data fitting.

[1] A. Pfitzner, *Chem. Eur. J.* **2000**, *6*, 1891–1898.
[2] M. H. Möller, W. Jeitschko, *J. Solid State Chem.* **1986**, *65*, 178–189.
[3] E. Freudenthaler, A. Pfizner, *Z. Kristallogr.* **1997**, *212*, 103–109.
[4] E. Freudenthaler, A. Pfitzner, *Angew. Chem.* **1995**, *107*, 1784–1786; *Angew. Chem. Int. Ed. Engl.* **1995**, *34*, 1647–1649.
[5] E. Freudenthaler, A. Pfitzner, *Z. Kristallogr.* **1995**, *210*, 59–59.
[6] E. Freudenthaler, A. Pfitzner, *Z. Naturforsch. B* **1997**, *52*, 199–202.
[7] E. Freudenthaler, A. Pfitzner, *Solid State Ionics* **1997**, *101–103*, 1053–1059.
[8] E. Freudenthaler, D. C. Sinclair, A. Pfitzner, *Mater. Res. Bull.* **1996**, *31*, 171–176.
[9] T. Takahashi, O. Yamamoto, S. Yamada, S. Hayashi, *J. Electrochem. Soc.* **1979**, *126*, 1654–1658.
[10] B. Jayasekera, J. A. Aitken, M. J. Heeg, S. L. Brock, *Inorg. Chem.* **2003**, *42*, 658–660.
[11] S. Böcker, M. Häser, *Z. Anorg. Allg. Chem.* **1995**, *621*, 258–286.
[12] H. Von Thurn, H. Krebs, *Acta Crystallogr. Sect. B* **1969**, *25*, 125–135.
[13] A. Pfitzner, M. F. Brau, J. Zweck, G. Brunklaus, H. Eckert, *Angew. Chem.* **2004**, *116*, 4324–4327; *Angew. Chem. Int. Ed.* **2004**, *43*, 4228–4231.
[14] B. Jayasekera, K. Somaskandan, S. L. Brock, *Inorg. Chem.* **2004**, *43*, 6902–6904.
[15] B. Jayasekera, S. L. Brock, *Mater. Res. Soc. Symp. Proc.* **2003**, *755*, DD6.12.1–6.12.6.
[16] G. Brunklaus, J. C. C. Chan, H. Eckert, *Z. Phys. Chem.* **2003**, *217*, 1627–1639.
[17] G. Maheut, M. Hervieu, C. Fernandez, V. Montouillout, D. Villemin, P. A. Jaffres, *J. Mol. Struct.* **2003**, *659*, 135–142.
[18] R. K. Harris, A. C. Olivieri, *Prog. Nucl. Magn. Reson. Spectrosc.* **1992**, *24*, 435–456.
[19] A. Olivieri, *J. Am. Chem. Soc.* **1992**, *114*, 5758–5763.
[20] R. W. Schurko, R. E. Wasylishen, J. H. Nelson, *J. Phys. Chem.* **1996**, *100*, 8057–8060.
[21] R. Blachnik, P. Lonnecke, J. Nuss, *Z. Naturforsch. B* **1993**, *48*, 1175–1180.
[22] L. Chai, A. Navrotsky, *Geochim. Cosmochim. Acta* **1996**, *60*, 4377–4383.
[23] L. Vegard, *Z. Phys.* **1921**, *5*, 17–26.
[24] M. J. Lambregts, S. Frank, *Talanta* **2004**, *62*, 627–630.
[25] W. Hönle, H. G. von Schnering, *Chem. Rev.* **1988**, *88*, 242–269.
[26] M. Baudler, *Angew. Chem.* **1987**, *99*, 429–451; *Angew. Chem. Int. Ed. Engl.* **1987**, *26*, 419–441.
[27] G. Brunklaus, J. C. C. Chan, H. Eckert, S. Reiser, T. Nilges, A. Pfitzner, *Phys. Chem. Chem. Phys.* **2003**, *5*, 3768–3776.
[28] K. C. Kao, W. Hwang, *Electrical Transport in Solids*, *Vol. 14*, Pergamon, Oxford, **1981**.
[29] C. J. F. Bottcher, P. Bordewijk, *Theory of Electric Polarization*, *Vol. II*, 2nd ed., Elsevier, Amsterdam, **1978**.
[30] N. E. Hill, W. E. Vanughan, A. H. Price, M. Davies, *Dielectric Properties and Molecular Behavior*, Van Nostrand Reinhold, London, **1969**.
[31] C. P. Grey, A. J. Vega, *J. Am. Chem. Soc.* **1995**, *117*, 8232–8242.
[32] S. Braun, H.-O. Kalinowski, S. Berger, *150 and More Basic NMR Experiments*, 2nd ed., Wiley-VCH, Weinheim, **1998**.

Received: July 15, 2004
Revised: January 31, 2005
Published online: April 13, 2005